ACS SENSORS

pubs.acs.org/acssensors

Letter

Photocontrolled Nanopipette Biosensor for ATP Gradient Electroanalysis of Single Living Cells

Si-Yuan Yu, Yi-Fan Ruan, Yi-Li Liu, De-Man Han,* Hong Zhou, Wei-Wei Zhao,* Dechen Jiang, Jing-Juan Xu, and Hong-Yuan Chen

Cite This: *ACS Sens.* 2021, 6, 1529–1535

Read Online

ACCESS | Metrics & More | Article Recommendations | Supporting Information

ABSTRACT: Emerging nanopipette tools have demonstrated substantial potential for advanced single-cell analysis, which plays vital roles from fundamental cellular biology to biomedical diagnostics. Highly recyclable nanopipettes with easy and quick regeneration are of special interest for precise and multiple measurements. However, existing recycle strategies are generally plagued by operational complexity and limited efficiency. Light, acting in a noncontact way, should be the ideal external stimulus to address this issue. Herein, we present the photocontrolled nanopipette capable of probing cellular adenosine triphosphate (ATP) gradient at single-cell level with good sensitivity, selectivity, and reversibility, which stems from the use of ATP-specific azobenzene (Azo)-incorporated DNA aptamer strands (AIDAS) and thereby the sensible transduction of variable nanopore size by the ionic currents passing through the aperture. Photoisomerized conformational change of the AIDAS by alternative UV/vis light stimulation ensures its noninvasive regeneration and repeated detection. Inducement and inhibition of the cellular ATP could also be probed by this nanosensor.

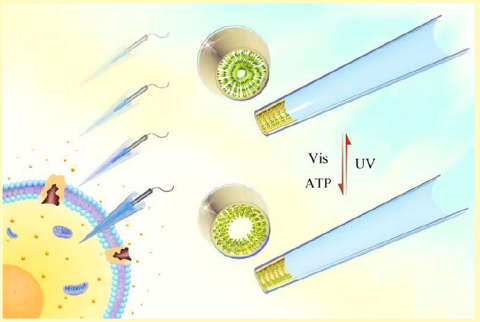

KEYWORDS: *nanopipette, photocontrol, azobenzene, single cell, electroanalysis, ATP*

Nanoelectrochemistry has been demonstrated as a powerful technology for deeper understanding of cell metabolism and cell heterogeneity.[1−10] Glass nanopipette represents a state-of-the-art approach for single-cell analysis. Its unique features in terms of fast fabrication, tunable orifice, and large cavity for customized filling/functionalization, as well as on-demand injection and aspiration, make possible intracellular manipulations and measurements with high temporal and spatial resolutions under different physicochemical principles.[11−25] Recently, for example, a double-barrel nanopipette served as minimally invasive nanotweezers for dielectrophoretic single-cell biopsies;[26] the plasmonic gold nanostars functionalized the nanopipette for Raman quantification of O_2 levels in hypoxic single cells;[27] the G-quadruplex (G4) DNA sequence was confined in an ultrasmall nanopipette with K^+-dependent conformational transformation for tracking stimulus-induced K^+ fluctuation under physiological conditions via resistive pulse;[28] and porous Pt was chemically deposited in a nanopipette for bipolar electrochemiluminescent detection of intracellular H_2O_2 and glucose.[29]

Nature has optimized biochannels capable of exquisite operation in response to external stimuli such as light, voltage, ions, and biomolecules, which has stimulated extensive efforts to develop artificial nanosystems mimicking biological activities.[30−36] Among various stimuli, light is especially attractive because it is noninvasive and permits bioorthogonal control of high spatiotemporal precision, and its noncontact operation would not cause any contamination into the nanosystems.[37−41] To correlate with light, light-responsive ion transport has been reported, on the basis of the photocontrolled change of surface charge and pore size within the nanochannels. For example, a light and pH dual-response ionic gate was constructed with the switch controlled by the surface charge[42] and a sulfonated spiropyran integrated metal−organic framework for photoswitchable proton transport based on effective pore size.[43] On the other hand, azobenzene (Azo), with interconvertable nonplanar *cis*- and planar *trans*-states upon UV/visible light irradiation, has often been employed as the essential photoswitch.[44−47] For instance, Azo-DNA integrated with graphene oxide mobilized a porous anodic alumina membrane for the rhodopsin-like photocontrolled gate of ion transport,[46] and Azo moieties attached fragaceatoxin C toxin for remote light control of the nanopore assembly.[47] However, the development of a light-responsive nanopipette has remained out of reach.

Motivated by the above arguments, this work described a photocontrolled nanopipette biosensor for single-cell electro-

Received: March 3, 2021
Accepted: April 12, 2021
Published: April 13, 2021

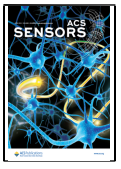

https://doi.org/10.1021/acssensors.1c00463
ACS Sens. 2021, 6, 1529−1535

analysis. Adenosine triphosphate (ATP), as the molecular unit of currency in all forms of life, not only provides energy to many cellular processes, e.g., nerve impulse propagation and muscle contraction, but also functions as signaling molecules for regulating, e.g., neurotransmission and ion channels.[48,49] Its detection has been actively pursued with various techniques.[50−58] Herein, by using the ATP-specific Azo-incorporated DNA aptamer strands (AIDAS),[44,45] the photocontrolled nanopipette was developed with high recyclability to ensure the cellular ATP gradient probing on the basis of ionic current. Specifically, a laser-pulled glass nanopipette was coated with gold (Au) layers on its interior walls and then modified with thiol-capped AIDAS photoswitch (Figure S1), which exhibited ATP/vis-dependent conformational transformation and UV-enabled recyclability (Figure S2) (see the Supporting Information for experimental details).

RESULTS AND DISCUSSION

Materials Characterization. As characterized by scanning electron microscopy (SEM), the glass nanopipette was laser-pulled with a small circular orifice of ca. 60 nm (Figure S3), which reduced to ca. 50 nm after sputtering the Au coating (Figure 1a), which was recognized with minimal invasiveness to a living single cell.[59] The interior Au coating was confirmed by focused ion beam (FIB) sculpture and elemental mapping.

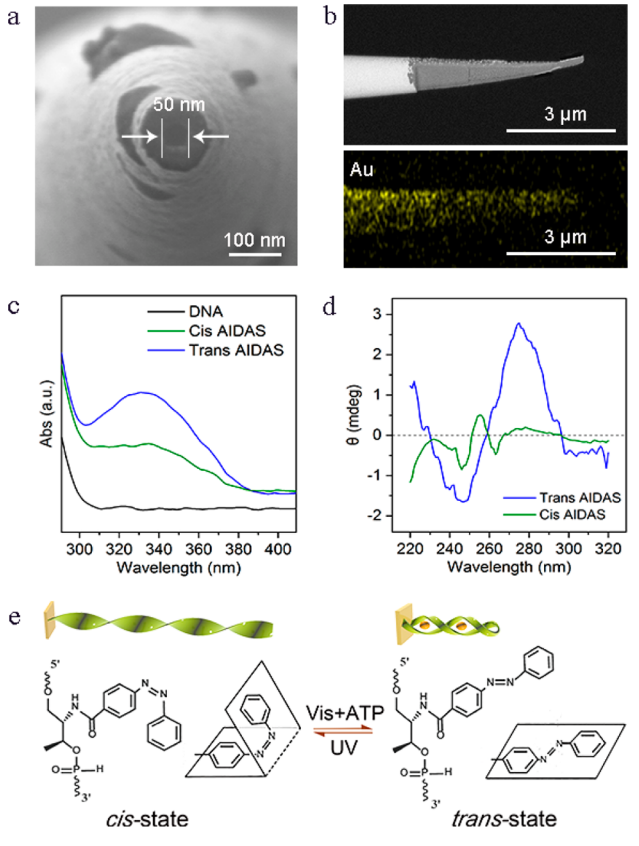

Figure 1. (a) Top-view SEM image of an Au-coated nanopipette with an orifice of ca. 50 nm. (b) SEM of a FIB-sculpted nanopipette (top) and corresponding Au mapping (bottom). (c) Absorbance spectra of DNA and AIDAS under different isomeric states. (d) CD spectra of AIDAS at ATP-free *cis*-states and ATP-binding *trans*-states. (e) Conformational change of AIDAS under *cis* (left) and *trans* (right) states. Structure-switch of AIDAS led to alternative capture and release of the ATP molecules.

A rough Au layer composed of small Au particles could be clearly observed within sculptured Au-coated nanopipette (Figure 1b top and Figure S4), and the even distribution of Si, O, and Au elements indicated the continuous deposition of interior Au layer (Figure 1b bottom and Figure S5). The ionic measurements at −1.0 V also validated the Au deposition (Figure S6). On the other hand, the photoisomerization process of AIDAS was investigated by the absorbance spectra. Compared to the spectrum of pristine DNA (black curve), a new peak appeared in the AIDAS (blue and green curves) (Figure 1c), and the spectrum difference between *trans*- and *cis*-AIDAS was caused by the two benzenes of the former being coplanar with the N═N double bond. Circular dichroism (CD) spectra of the ATP-contained *trans*-AIDAS (blue curve) was different from that of ATP-free *cis* one (green curve); the obvious positive (at ca. 275 nm) and negative (at ca. 245 nm) bands appeared in that of ATP-contained *trans*-AIDAS (Figure 1d), because the planar *trans*-Azo in the DNA backbone could stabilize the DNA duplex by base stacking to form a hairpin structure, which could be further stabilized by capturing ATP molecules (Figure 1e).[44]

Feasibility Study. The open-circuit potential (OCP) was performed to compare the Au-coated nanopipette and AIDAS functionalized one (denoted as AIDAS-NP) using the illustrated setup (Figure 2a inset). The dramatic OCP change confirmed the successful functionalization of the AIDAS within the nanopipette (Figure 2a). With UV/vis light irradiation as external stimuli, ATP capture was performed by immersing the *cis*-AIDAS-NP into ATP-containing solution for 10 s under visible light (450 nm) illumination for 2 min to complete the conformational transformation, and then the ionic measurements were conducted in 20 mM ATP-free Tris-HCl solution containing 40 mM KCl, and the regeneration from the *trans*-AIDAS-NP was made by UV light (365 nm) treatment for 2 min, while keeping the bias at +3.0 V to eject the released ATP out of the nanotip.[15] The ionic current rectification (ICR) was then studied. As shown, the Au-coated nanopipette exhibited relatively strong rectification characteristics due to adsorption of numerous anions (Cl^-) (Figure 2b, red curve). Here, the AIDAS-induced increase of the negative surface charge yet caused a decrease in the rectification degree, probably due to the large physical size of AIDAS. Besides, the ATP-free *cis*-AIDAS induced a smaller rectification ratio (Figure 2b, green curve) than that of ATP-contained *trans*-AIDAS (Figure 2b, blue curve). This revealed that the AIDAS conformational change, rather than surface charge on the interior wall, dominated the ion transport through the orifice. The overall rectification ratios of the corresponding change were calculated (Figure 2b inset). The resistance-pulse measurement ($i-t$ curve) could directly reflect the nanopipette state via the magnitude of ionic currents.[60−62] In the present case, the ATP-free *cis*-AIDAS and ATP-binding *trans*-AIDAS generated distinct ionic responses at the voltage of −1.0 V (Figure 2c), which confirmed the dominance of AIDAS conformation in this phenomenon, i.e., the single-stranded configuration of *cis*-AIDAS could increase the blockade of the nanopipette (decrease the effective pore size) that inhibited the ion transport, whereas the stable hairpin structure of *trans*-AIDAS could increase the effective pore size allowing larger ionic current (Figure 2c inset). Moreover, the control experiment of AIDAS-NP irradiated with UV/vis light under no ATP treatment further validated the feasibility of the biosensor (Figure S7).

https://doi.org/10.1021/acssensors.1c00463
ACS Sens. 2021, 6, 1529−1535

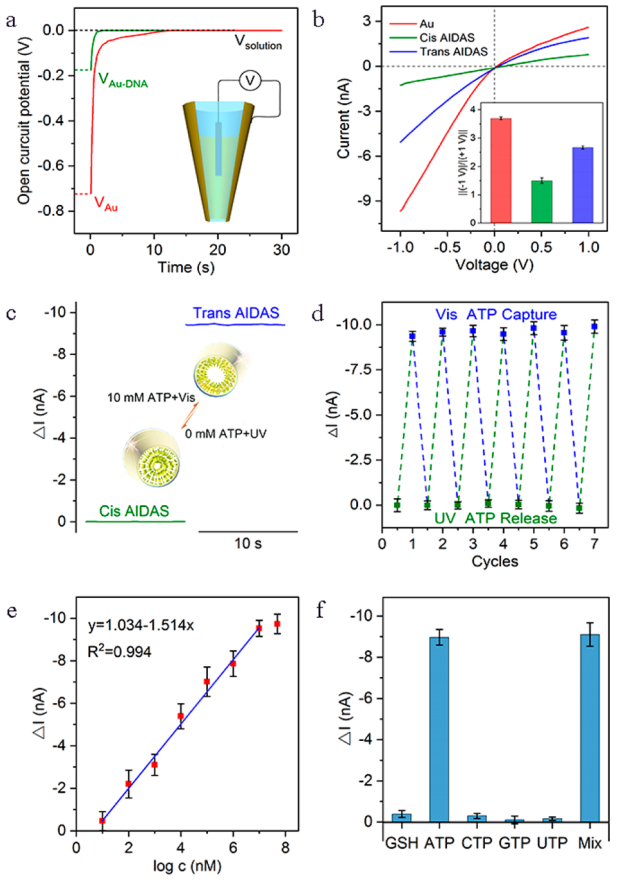

Figure 2. (a) OCP measurements. Inset: the setup using an as-evaporated nanopipette with Au layers on both interior and exterior walls; an Ag/AgCl wire electrode inserted in the capillary that connected to the Au layer on the exterior wall. With backfilled solution, the nanopipette was held in air, thereby generating a reaction chamber at the nanopit tip for studying the interior surface. (b) Obtained *I*−*V* curves of the AIDAS at *cis* and *trans* states. Inset: corresponding ICR ratio. (c) Obtained *I*−*V* curves of *cis*-AIDAS with UV light and *trans*-AIDAS with ATP and visible light. Inset: schematic of the conformational change of photocontrolled AIDAS in the nanopipette. (d) Photocontrolled recyclability of the AIDAS-NP. (e) Increased ionic currents as the enhanced ATP concentration. (f) Selectivity test. Note: Δ*I* represents the difference of ionic signals at −1.0 V between before (*cis*-AIDAS) and after (*trans*-AIDAS) ATP capture.

Biosensor Performance. The amount of *cis*-AIDAS was in advance optimized to achieve the maximal blockade effect and protect the nanodevice from the interference of thiols (Figure S8). Furthermore, since the wireless Au-coated electrode may be polarized under the external electrical field, common redox mediators in the cytoplasm may impact the ionic signals.[63,64] Hence, $Fe(CN)_6^{3-/4-}$ were used as an example for the corresponding investigation. As shown in the obtained *I*−*V* curves (Figure S9), no distinct redox peaks and offset of ionic signals were observed due to the good blockade effect of AIDAS, indicating elimination of any possible effect of Au polarization. Incidentally, sampling time of ATP for 10 s was determined to be sufficient for ATP binding (Figure S10). For repeated ATP release and capture, stable signal recovery was observed, suggesting the excellent photocontrolled reversibility of the nanodevice (Figure 2d). Parallel signals from 12 nanopipettes in the same batch demonstrated high precision and reproducibility (Figure S11). The effect of ATP concentrations on differential ionic responses of AIDAS-NP were also studied. As shown, the signals increased with the enhanced ATP concentrations, indicating formation of more ATP-binding *trans*-AIDAS within the nanopipette, which displayed a good linear relationship between Δ*I* and the logarithm of ATP concentration approximately from 10 nM to 10 mM (Figure 2e). This phenomenon coincided with multiple gating states in a single conical nanochannel.[65] Then, selectivity was studied by using glutathione (GSH) and ATP analogues of uridine triphosphate (UTP), guanidine triphosphate (GTP), as well as cytosine triphosphate (CTP) as the interfering substances with equivalent concentration of ATP. Ionic current responses from these species were similar to the blank solution and much lower than that of ATP and mixture, demonstrating its high specificity toward ATP (Figure 2f). Besides, according to previous studies,[58] adenosine diphosphate sodium salt (ADP), adenosine monophosphate (AMP), and adenosine could cross react with the ATP aptamers (Figure S12, red bars). Nevertheless, the mixed solution including 5 mM ATP and interferents (0.15 mM ADP, 0.1 mM AMP, 0.5 μM adenosine), whose concentrations were set according to the actual intracellular content,[66] generated similar ionic signals at −1.0 V to those of bare 5 mM ATP, indicating the minimal effect on cellular ATP detection (Figure S12, blue bar).

Cellular ATP Gradient Detection. The AIDAS-NP was then applied for probing local cellular ATP concentration and its gradient of the individual H9C2 cardiac myoblasts, with the assistance of a three-dimensional (3D) micromanipulator to approach and penetrate the myoblasts at different heights in *z* dimension. Notably, ultrasporadic cells were cultured for avoiding interference from adjacent cells during measurement (Figure S13). Presumably, the myoblasts could generate a gradient from the intracellular cytoplasm to the nearby medium. Four positions, i.e., ca. 1500 μm, ca. 750 μm, ca. 10 μm, and −2 μm relative to the cell membrane, were selected for cellular ATP gradient electrochemical measurements (Figure 3a). The contact between the nanotip and the cell membrane could be sensitively reflected through the ion current signals; i.e., the baseline current of the nanopipette would instantaneously drop with the bias of +0.3 V (Figure S14). In addition, the dimple of the cell membrane could be observed at the contact point by a microscope field (40×) (Figure S15). Then, by adjusting the relative altitude of AIDAS-NP, the vertical probing process (from far to near) of the four positions was performed with the focus of the microscope on the nanotip (Figure 3b). Incidentally, the insertion into the target cell was also confirmed by the change of ionic signals (Figure S16). At different positions, variable ionic current magnitudes were observed, and recording of ionic signals was sequentially repeated 8 times (Figure 3c). Generally, the ionic current intensity increased with smaller distance, and the intracellular values exhibited a large enhancement as compared to the extracellular results, indicating high ATP concentration in the cytoplasm. No cellular morphology change was observed after the repeated detection, suggesting that the nanodevice had no effect against the cell viability.[20] Under the same conditions, detection of 12 individual cells was also performed with minor signal variation (Figure 3d). Together, these results evidenced that the ionic current magnitudes of AIDAS-NP associated intimately with ATP-provoked gating states and its feasibility for probing cellular ATP gradient. Incidentally, the nanosensor was

https://doi.org/10.1021/acssensors.1c00463
ACS Sens. 2021, 6, 1529−1535

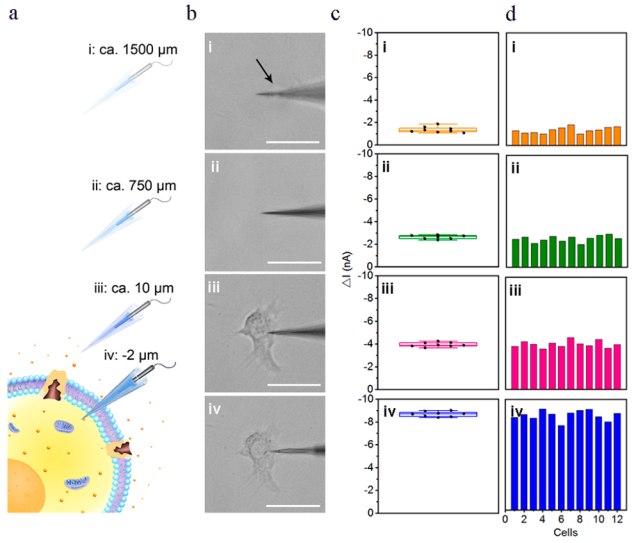

Figure 3. (a) Probing cellular ATP gradient by approaching AIDAS-NP to a target cell in *z* dimension. The nanosized tip allowed easy and multiple insertion into the cytosol, and the orange dots distributed across the cell membrane represent the ATP molecules. (b) AIDAS-NP at the four distances with the focal plane of the microscopy focused on the nanotip. Note: black arrow points to the liquid level. The scale bars represent 50 μm. (c) Repeated ionic current magnitudes at different positions. (d) Corresponding statistical studies with 12 individual cells.

recovered before each measurement to guarantee its identical initial response.

External Stimuli. Due to the serious biochemical consequences of deficiency or excess of important endogenous species, research on drug effects on cellular status is important. The potential of AIDAS-NP for probing such effects was exemplified by Ca^{2+}-provoked ATP inducement and oligomycin-inhibited ATP depletion,[67] with the use of JC-1, a cationic lipophilic dye reflecting the mitochondrial membrane potential ($\Delta\Psi m$),[68] to indicate the intracellular ATP production (Figure 4a). For normal cells, high $\Delta\Psi m$ facilitates the accumulation of JC-1 monomers (J-monomers) in the mitochondrion to form corresponding complexes (J-aggregates) emitting strong red fluorescence. However, lower $\Delta\Psi m$ would go against the

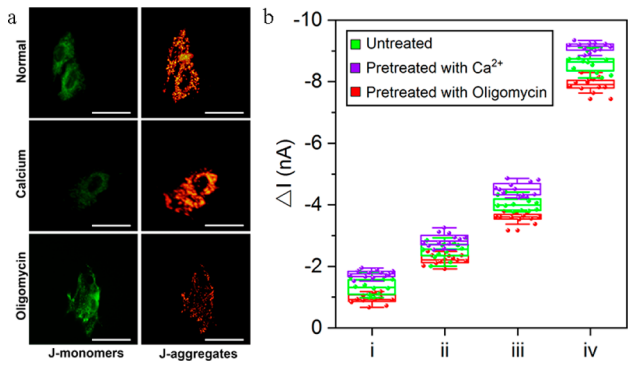

Figure 4. (a) Fluorescent images of JC-1 stained H9C2 cardiac myoblasts with calcium, oligomycin, and no treatment for the characterization of mitochondrial function. The scale bars represent 50 μm, and the exposure time was set as 0.5 s. (b) Ionic current responses collected at −1.0 V from 12 individual cells with normal, calcium, and oligomycin treatment, respectively.

accumulation of J-monomers, and most of them in the cytoplasm would emit shorter green wavelength florescence. Compared to the normal cardiac myoblasts, as shown, Ca^{2+}-treated myoblasts exhibited stronger red fluorescence from J-aggregates and weaker green fluorescence from the J-monomers. By contrast, a converse phenomenon was observed in the oligomycin-treated myoblasts. Then, measurements on single normal/Ca^{2+}-provoked/oligomycin-inhibited myoblasts were repeated 8 times (Figure S17), and measurements on 12 individual myoblasts were also performed (Figure 4b). Comparatively, the corresponding ionic currents collected at the four positions of Ca^{2+}-treated myoblasts exhibited a distinct increment compared to those from untreated H9C2 cardiac myoblasts, whereas obvious lower ionic currents were observed for oligomycin-treated myoblasts. Via the Ca^{2+}-provoked ATP inducement and oligomycin-inhibited ATP depletion effects, these results revealed the potency of AIDAS-NP to probe ATP fluctuation from respective drug therapies.

CONCLUSIONS

In this work, a photocontrolled recyclable nanopipette tool was demonstrated for sensitive probing of cellular ATP gradient. Light assisted ATP-dependent gating status at the confined nanotip could be sensibly transduced by the ionic response, and the on-demand conformational change of AIDAS photoswitched by alternate UV/vis light allowed the short regeneration time of the nanodevice. By comparing with all existing studies using the confined nanopores (Table S1), we believe this work timely complemented other efforts in the nanopipette community for single-cell analysis. Light, with many other potential photoswitches (e.g., includediarylethenes,[69] spiropyrans,[70] triphenylmethane leuco derivatives,[71] fulgide,[72] and alkenes[73]), is highly expected to further advance the development of photocontrolled nanopipettes capable of versatile applications.

ASSOCIATED CONTENT

Supporting Information

The Supporting Information is available free of charge at https://pubs.acs.org/doi/10.1021/acssensors.1c00463.

Additional details on materials and experimental methods; Illustrations of nanopipettes pulling and Au coating, fabrication of the AIDAS-NP, photoswitching of AIDAS-NP, FIB and setup for cellular ATP recording; SEM image of the FIB-process nanopipette and corresponding element mapping; Effect of inner-wall Au polarization; Signal optimization; Selectivity effect of ADP, AMP, and adenosine; Parallel signals obtained by 12 nanopipettes; Signals change when the nanopipette contacted and penetrated the cell membrane; Image of highly sporadic H9C2 myoblasts; Eight times repeated measurements on single untreated and drug treated cells; Comparsion of nanopipette single-cell electroanalysis using the confined nanopores (PDF)

AUTHOR INFORMATION

Corresponding Authors

De-Man Han − *Engineering Research Center of Recycling & Comprehensive Utilization of Pharmaceutical and Chemical Waste of Zhejiang Province, Taizhou University, Jiaojiang 318000, China;* orcid.org/0000-0003-1995-0770; Email: hdm@tzc.edu.cn

https://doi.org/10.1021/acssensors.1c00463
ACS Sens. 2021, 6, 1529−1535

Wei-Wei Zhao − *State Key Laboratory of Analytical Chemistry for Life Science, School of Chemistry and Chemical Engineering, Nanjing University, Nanjing 210093, China;* orcid.org/0000-0002-8179-4775; Email: zww@nju.edu.cn

Authors

Si-Yuan Yu − *State Key Laboratory of Analytical Chemistry for Life Science, School of Chemistry and Chemical Engineering, Nanjing University, Nanjing 210093, China*

Yi-Fan Ruan − *State Key Laboratory of Analytical Chemistry for Life Science, School of Chemistry and Chemical Engineering, Nanjing University, Nanjing 210093, China*

Yi-Li Liu − *State Key Laboratory of Analytical Chemistry for Life Science, School of Chemistry and Chemical Engineering, Nanjing University, Nanjing 210093, China*

Hong Zhou − *Shandong Key Laboratory of Biochemical Analysis, College of Chemistry and Molecular Engineering, Qingdao University of Science and Technology, Qingdao 266042, China;* orcid.org/0000-0002-9264-7148

Dechen Jiang − *State Key Laboratory of Analytical Chemistry for Life Science, School of Chemistry and Chemical Engineering, Nanjing University, Nanjing 210093, China;* orcid.org/0000-0002-2845-3621

Jing-Juan Xu − *State Key Laboratory of Analytical Chemistry for Life Science, School of Chemistry and Chemical Engineering, Nanjing University, Nanjing 210093, China;* orcid.org/0000-0001-9579-9318

Hong-Yuan Chen − *State Key Laboratory of Analytical Chemistry for Life Science, School of Chemistry and Chemical Engineering, Nanjing University, Nanjing 210093, China*

Complete contact information is available at: https://pubs.acs.org/10.1021/acssensors.1c00463

Notes

The authors declare no competing financial interest.

■ ACKNOWLEDGMENTS

We thank Y. F. Xiong for helping with FIB sculpture. This work is well supported by National Natural Science Foundation of China (Grant Nos. 21675080, 21976129, and 21974059), Natural Science Foundation of Jiangsu Province (Grant BK20170073), and Excellent Research Program of Nanjing University (ZYJH004).

■ REFERENCES

(1) Wightman, R. Probing Cellular Chemistry in Biological Systems with Microelectrodes. *Science* **2006**, *311*, 1570−1574.

(2) Amatore, C.; Arbault, S.; Guille, M.; Lemaitre, F. Electrochemical Monitoring of Single Cell Secretion: Vesicular Exocytosis and Oxidative Stress. *Chem. Rev.* **2008**, *108*, 2585−2621.

(3) Sun, P.; Laforge, F. O.; Abeyweera, T. P.; Rotenberg, S. A.; Carpino, J.; Mirkin, M. V. Nanoelectrochemistry of Mammalian Cells. *Proc. Natl. Acad. Sci. U. S. A.* **2008**, *105*, 443−448.

(4) Li, X.; Majdi, S.; Dunevall, J.; Fathali, H.; Ewing, A. G. Quantitative Measurement of Transmitters in Individual Vesicles in the Cytoplasm of Single Cells with Nanotip Electrodes. *Angew. Chem., Int. Ed.* **2015**, *54*, 11978−11982.

(5) Li, X.; Dunevall, J.; Ewing, A. G. Quantitative Chemical Measurements of Vesicular Transmitters with Electrochemical Cytometry. *Acc. Chem. Res.* **2016**, *49*, 2347−2354.

(6) Zhang, X.-W.; Qiu, Q.-F.; Jiang, H.; Zhang, F.-L.; Liu, Y.-L.; Amatore, C.; Huang, W.-H. Real-Time Intracellular Measurements of ROS and RNS in Living Cells with Single Core-Shell Nanowire Electrodes. *Angew. Chem., Int. Ed.* **2017**, *56*, 12997−13000.

(7) Li, Y.; Hu, K.; Yu, Y.; Rotenberg, S. A.; Amatore, C.; Mirkin, M. V. Direct Electrochemical Measurements of Reactive Oxygen and Nitrogen Species in Non-Transformed and Metastatic Human Breast Cells. *J. Am. Chem. Soc.* **2017**, *139*, 13055−13062.

(8) Hu, K.; Li, Y.; Rotenberg, S. A.; Amatore, C.; Mirkin, M. V. Electrochemical Measurements of Reactive Oxygen and Nitrogen Species inside Single Phagolysosomes of Living Macrophages. *J. Am. Chem. Soc.* **2019**, *141*, 4564−4568.

(9) Zhu, W.; Gu, C.; Dunevall, J.; Ren, L.; Zhou, X.; Ewing, A. G. Combined Amperometry and Electrochemical Cytometry Reveal Differential Effects of Cocaine and Methylphenidate on Exocytosis and the Fraction of Chemical Release. *Angew. Chem., Int. Ed.* **2019**, *58*, 4238−4242.

(10) Zhang, X.-W.; Oleinick, A.; Jiang, H.; Liao, Q.-L.; Qiu, Q.-F.; Svir, I.; Liu, Y.-L.; Amatore, C.; Huang, W.-H. Electrochemical Monitoring of ROS/RNS Homeostasis Within Individual Phagolysosomes Inside Single Macrophages. *Angew. Chem., Int. Ed.* **2019**, *58*, 7753−7756.

(11) Son, D.; Park, S. Y.; Kim, B.; Koh, J. T.; Kim, T. H.; An, S.; Jang, D.; Kim, G. T.; Jhe, W.; Hong, S. Nanoneedle Transistor-Based Sensors for the Selective Detection of Intracellular Calcium Ions. *ACS Nano* **2011**, *5*, 3888−3895.

(12) Actis, P.; Maalouf, M. M.; Kim, H. J.; Lohith, A.; Vilozny, B.; Seger, R. A.; Pourmand, N. Compartmental Genomics in Living Cells Revealed by Single-Cell Nanobiopsy. *ACS Nano* **2014**, *8*, 546−553.

(13) Nashimoto, Y.; Takahashi, Y.; Zhou, Y.; Ito, H.; Ida, H.; Ino, K.; Matsue, T.; Shiku, H. Evaluation of mRNA Localization Using Double Barrel Scanning Ion Conductance Microscopy. *ACS Nano* **2016**, *10*, 6915−6922.

(14) Nascimento, R. A. S.; Özel, R. E.; Mak, W. H.; Mulato, M.; Singaram, B.; Pourmand, N. Single Cell 'Glucose Nanosensor' Verifies Elevated Glucose Levels in Individual Cancer Cells. *Nano Lett.* **2016**, *16*, 1194−1200.

(15) Pan, R.; Xu, M.; Jiang, D.; Burgess, J. D.; Chen, H. Y. Nanokit for Single-Cell Electrochemical Analyses. *Proc. Natl. Acad. Sci. U. S. A.* **2016**, *113*, 11436−11440.

(16) Ying, Y. L.; Li, Y. J.; Mei, J.; Gao, R.; Hu, Y. X.; Long, Y. T.; Tian, H. Manipulating and Visualizing the Dynamic Aggregation-Induced Emission within a Confined Quartz Nanopore. *Nat. Commun.* **2018**, *9*, 3657.

(17) Liu, H.; Jiang, Q.; Pang, J.; Jiang, Z.; Cao, J.; Ji, L.; Xia, X.; Wang, K. A Multiparameter pH-Sensitive Nanodevice Based on Plasmonic Nanopores. *Adv. Funct. Mater.* **2018**, *28*, 1703847.

(18) Ying, Y. L.; Hu, Y. X.; Gao, R.; Yu, R. J.; Gu, Z.; Lee, L. P.; Long, Y. T. Asymmetric Nanopore Electrode-Based Amplification for Electron Transfer Imaging in Live Cells. *J. Am. Chem. Soc.* **2018**, *140*, 5385−5392.

(19) Özel, R. E.; Bulbul, G.; Perez, J.; Pourmand, N. Functionalized Quartz Nanopipette for Intracellular Superoxide Sensing: A Tool for Monitoring Reactive Oxygen Species Levels in Single Living Cell. *ACS Sens.* **2018**, *3*, 1316−1321.

(20) Song, J.; Xu, C. H.; Huang, S. Z.; Lei, W.; Ruan, Y. F.; Lu, H. J.; Zhao, W.; Xu, J. J.; Chen, H. Y. Ultrasmall Nanopipette: Toward Continuous Monitoring of Redox Metabolism at Subcellular Level. *Angew. Chem., Int. Ed.* **2018**, *57*, 13226−13230.

(21) Wang, X. Y.; Wilkinson, M. D.; Lin, X. Y.; Ren, R.; Willison, K. R.; Ivanov, A. P.; Jake, B.; Edel, J. B. Single-Molecule Nanopore Sensing of Actin Dynamics and Drug Binding. *Chem. Sci.* **2020**, *11*, 970−979.

(22) Chen, W. T.; Ding, S.; Wu, J. R.; Shi, G. Y.; Zhu, A. W. In Situ Detection of Hydroxyl Radicals in Mitochondrial Oxidative Stress with a Nanopipette Electrode. *Chem. Commun.* **2020**, *56*, 13225−13228.

(23) Li, Z. Y.; Liu, Y.; Li, Y. J.; Wang, W. H.; Song, Y.; Zhang, J.; Tian, H. High-preservation Single-cell Operation through a Photo-responsive Hydrogel-Nanopipette System. *Angew. Chem., Int. Ed.* **2021**, *60*, 5157.

(24) Pan, R. R.; Hu, K. K.; Jia, R.; Rotenberg, S. A.; Jiang, D.; Mirkin, M. V. Resistive-Pulse Sensing Inside Single Living Cells. *J. Am. Chem. Soc.* **2020**, *142*, 5778−5784.
(25) Hu, K. K.; Jia, R.; Hatamie, A.; Vo, K.; Mirkin, M. V.; Ewing, A. G. Correlating Molecule Count and Release Kinetics with Vesicular Size Using Open Carbon Nanopipettes. *J. Am. Chem. Soc.* **2020**, *142*, 16910−16914.
(26) Nadappuram, B. P.; Cadinu, P.; Barik, A.; Ainscough, A. J.; Devine, M. J.; Kang, M.; Garcia, J. G.; Kittler, J. T.; Willison, K. R.; Vilar, R.; Actis, P.; Stothard, B. W.; Oh, S. H.; Ivanov, A. P.; Edel, J. B. Nanoscale Tweezers for Single-Cell Biopsies. *Nat. Nanotechnol.* **2019**, *14*, 80−88.
(27) Nguyen, T. D.; Song, M. S.; Ly, N. H.; Lee, S. Y.; Joo, S. W. Nanostars on Nanopipette Tips: A Raman Probe for Quantifying Oxygen Levels in Hypoxic Single Cells and Tumours. *Angew. Chem., Int. Ed.* **2019**, *58*, 2710−2714.
(28) Shi, X. M.; Ruan, Y. F.; Wang, H. Y.; Zhao, W. W.; Xu, J. J.; Chen, H. Y. A Supersmall Single-Cell Nanosensor for Intracellular K^+ Detection. *CCS Chem.* **2020**, *2*, 2359−2367.
(29) Wang, Y.; Jin, R.; Sojic, N.; Jiang, D.; Chen, H. Y. Intracellular Wireless Analysis of Single Cells by Bipolar Electrochemiluminescence Confined in a Nanopipette. *Angew. Chem., Int. Ed.* **2020**, *59*, 10416−10420.
(30) Casey, J. R.; Grinstein, S.; Orlowski, J. Sensors and Regulators of Intracellular pH. *Nat. Rev. Mol. Cell Biol.* **2010**, *11*, 50−61.
(31) Matsuyama, S.; Llopis, J.; Deveraux, Q. L.; Tsien, R. Y.; Reed, J. C. Changes in Intramitochondrial and Cytosolic pH: Early Events that Modulate Caspase Activation During Apoptosis. *Nat. Cell Biol.* **2000**, *2*, 318−325.
(32) Paroutis, P.; Touret, N.; Grinstein, S. The pH of the Secretory Pathway: Measurement, Determinants, and Regulation. *Physiology* **2004**, *19*, 207−215.
(33) Xiao, K.; Kong, X. Y.; Zhang, Z.; Xie, G.; Wen, L.; Jiang, L. Construction and Application of Photoresponsive Smart Nanochannels. *J. Photochem. Photobiol., C* **2016**, *26*, 31−47.
(34) Pérez-Mitta, G.; Peinetti, A. S.; Lorena, C. M.; Toimil, M. E.; Trautmann, C.; Azzaroni, O. Highly Sensitive Biosensing with Solid-State Nanopores Displaying Enzymatically Reconfigurable Rectification Properties. *Nano Lett.* **2018**, *18*, 3303−3310.
(35) Ding, D.; Gao, P.; Ma, Q.; Wang, D.; Xia, F. Biomolecule Functionalized Solid-State Ion Nanochannels/Nanopores: Features and Techniques. *Small* **2019**, *15*, 1804878.
(36) Sun, Y.; Chen, S.; Chen, X.; Xu, Y.; Zhang, S.; Ouyang, Q.; Yang, G.; Li, H. A Highly Selective and Recyclable NO-Responsive Nanochannel Based on a Spiroring Opening−Closing Reaction Strategy. *Nat. Commun.* **2019**, *10*, 1323.
(37) Mayer, G.; Heckel, A. Biologically Active Molecules with a "Light Switch. *Angew. Chem., Int. Ed.* **2006**, *45*, 4900−4921.
(38) Velema, W. A.; Szymanski, W.; Feringa, B. L. Photopharmacology: Beyond Proof of Principle. *J. Am. Chem. Soc.* **2014**, *136*, 2178−2191.
(39) Hüll, K.; Morstein, J.; Trauner, D. In Vivo Photopharmacology. *Chem. Rev.* **2018**, *118*, 10710−10747.
(40) Kuzyk, A.; Yang, Y.; Duan, X.; Stoll, S.; Govorov, A. O.; Sugiyama, H.; Endo, M.; Liu, N. A Light-Driven Three-Dimensional Plasmonic Nanosystem that Translates Molecular Motion into Reversible Chiroptical Function. *Nat. Commun.* **2016**, *7*, 10591.
(41) Lerch, M. M.; Hansen, M. J.; Van-Dam, G. M.; Szymanski, W.; Feringa, B. L. Emerging Targets in Photopharmacology. *Angew. Chem., Int. Ed.* **2016**, *55*, 10978−10999.
(42) Xiao, K.; Xie, G. H.; Li, P.; Liu, Q.; Hou, G. L.; Zhang, Z.; Ma, J.; Tian, Y.; Wen, L. P.; Jiang, L. A Biomometic Multi-Stimuli-Response Ionic Gate Using a Hydroxypyrene Derivation-Functionalized Asymmetric Single Nanochannel. *Adv. Mater.* **2014**, *26*, 6560−6565.
(43) Liang, H. Q.; Guo, Y.; Shi, Y. S.; Peng, X. S.; Liang, B.; Chen, B. L. A Light-Responsive Metal−Organic Framework Hybrid Membrane with High On/Off Photoswitchable Proton Conductivity. *Angew. Chem., Int. Ed.* **2020**, *59*, 7732−7737.
(44) Li, P.; Xie, G.; Liu, P.; Kong, X. Y.; Song, Y.; Wen, L. P.; Jiang, L. Light-Driven ATP Transmembrane Transport Controlled by DNA Nanomachines. *J. Am. Chem. Soc.* **2018**, *140*, 16048−16052.
(45) Asanuma, H.; Ito, T.; Yoshida, T.; Liang, X. G.; Komiyama, M. Photoregulation of the Formation and Dissociation of a DNA Duplex by Using the cis-trans Isomerization of Azobenzene. *Angew. Chem., Int. Ed.* **1999**, *38*, 2393−2395.
(46) Shi, L.; Mu, C.; Gao, T.; Chai, W.; Sheng, A.; Chen, T.; Yang, J.; Zhu, X.; Li, G. X. Rhodopsin-Like Ionic Gate Fabricated with Graphene Oxide and Isomeric DNA Switch for Efficient Photocontrol of Ion Transport. *J. Am. Chem. Soc.* **2019**, *141*, 8239−8243.
(47) Mutter, N. L.; Volarić, J.; Szymanski, W.; Feringa, B. L.; Maglia, G. Reversible Photocontrolled Nanopore Assembly. *J. Am. Chem. Soc.* **2019**, *141*, 14356−14363.
(48) Davalos, D.; Grutzendler, J.; Yang, G.; Kim, J. V.; Zuo, Y.; Jung, S.; Littman, D. R.; Dustin, M. L.; Gan, W. B. ATP Mediates Rapid Microglial Response to Local Brain Injury In. *Nat. Neurosci.* **2005**, *8*, 752−758.
(49) Hardie, D. G.; Ross, F. A.; Hawley, S. A. AMPK: A Nutrient and Energy Sensor that Maintains Energy Homeostasis. *Nat. Rev. Mol. Cell Biol.* **2012**, *13*, 251−262.
(50) Tian, J.; Zeng, X.; Xie, X.; Han, S.; Liew, O. W.; Chen, Y. T.; Wang, L.; Liu, X. Intracellular Adenosine Triphosphate Deprivation through Lanthanide-Doped Nanoparticles. *J. Am. Chem. Soc.* **2015**, *137*, 6550−6558.
(51) Zhang, Y.; Clausmeyer, J.; Babakinejad, B.; Lopez, A. C.; Ali, T.; Shevchuk, A.; Takahashi, Y.; Novak, P.; Edwards, C.; Lab, M.; Gopal, S.; Chiappini, C.; Anand, U.; Magnani, L.; Coombes, C.; Gorelik, J.; Matsue, T.; Schuhmann, W.; Klenerman, D.; Sviderskaya, E. V.; Korchev, Y. Spearhead Nanometric Field-Effect Transistor Sensors for Single-Cell Analysis. *ACS Nano* **2016**, *10*, 3214−3221.
(52) Wang, L.; Yuan, L.; Zeng, X.; Peng, J.; Ni, Y.; Er, J. C.; Xu, W.; Agrawalla, B. K.; Su, D.; Kim, B.; Chang, Y. T. A Multisite-Binding Switchable Fluorescent Probe for Monitoring Mitochondrial ATP Level Fluctuation in Live Cells. *Angew. Chem., Int. Ed.* **2016**, *55*, 1773−1776.
(53) Zhang, K. L.; He, X. L.; Liu, Y.; Yu, P.; Fei, J.; Mao, L. Highly Selective Cerebral ATP Assay Based on Micrometer Scale Ion Current Rectification at Polyimidazolium-Modified Micropipettes. *Anal. Chem.* **2017**, *89*, 6794−6799.
(54) Deng, J.; Wang, K.; Wang, M.; Yu, P.; Mao, L. Q. Mitochondria Targeted Nanoscale Zeolitic Imidazole Framework-90 for ATP Imaging in Live Cells. *J. Am. Chem. Soc.* **2017**, *139*, 5877−5882.
(55) Zhang, K. L.; Xiong, T. Y.; Wu, F.; Yue, Q. W.; Ji, W. L.; Yu, P.; Mao, L. Q. Real-Time and In-Situ Intracellular ATP Assay with Polyimidazolium Brush-Modified Nanopipette. *Sci. China: Chem.* **2020**, *63*, 1004−1011.
(56) Arai, S.; Kriszt, R.; Harada, K.; Looi, L. S.; Matsuda, S.; Wongso, D.; Suo, S.; Ishiura, S.; Tseng, Y. H.; Raghunath, M.; Ito, T.; Tsuboi, T.; Kitaguchi, T. RGB-Color Intensiometric Indicators to Visualize Spatiotemporal Dynamics of ATP in Single Cells. *Angew. Chem.* **2018**, *130*, 11039−11044.
(57) Di, Z.; Zhao, J.; Chu, H.; Xue, W.; Zhao, Y.; Li, L. An Acidic Microenvironment Driven DNA Nanomachine Enables Specific ATP Imaging in the Extracellular Milieu of Tumor. *Adv. Mater.* **2019**, *31*, 1901885.
(58) Wang, D. D.; Qi, G.; Zhou, Y.; Zhang, Y.; Wang, B.; Hu, P.; Jin, Y. D. Single-Cell ATP Detection and Content Analyses in Electrostimulus-Induced Apoptosis Using Functionalized Glass Nanopipettes. *Chem. Commun.* **2020**, *56*, 1561−1564.
(59) Chiappini, C. Nanoneedle-Based Sensing in Biological Systems. *ACS Sens.* **2017**, *2*, 1086−1102.
(60) Carson, S.; Wick, S. T.; Carr, P. A.; Wanunu, M.; Aguilar, C. A. Direct Analysis of Gene Synthesis Reactions Using Solid-State Nanopores. *ACS Nano* **2015**, *9*, 12417−12424.
(61) German, S. R.; Hurd, T. S.; White, H. S.; Mega, T. L. Sizing Individual Au Nanoparticles in Solution with Sub-Nanometer Resolution. *ACS Nano* **2015**, *9*, 7186−7194.

https://doi.org/10.1021/acssensors.1c00463
ACS Sens. 2021, 6, 1529−1535

(62) Li, T.; He, X.; Zhang, K.; Wang, K.; Yu, P.; Mao, L. Observing Single Nanoparticle Events at the Orifice of a Nanopipette. *Chem. Sci.* **2016**, *7*, 6365−6368.
(63) Ranallo, S.; Amodio, A.; Idili, A.; Porchetta, A.; Ricci, F. Electronic Control of DNA-Based Nanoswitches and Nanodevices. *Chem. Sci.* **2016**, *7*, 66−71.
(64) Wang, D.; Mirkin, M. V. Electron-Transfer Gated Ion Transport in Carbon Nanopipets. *J. Am. Chem. Soc.* **2017**, *139*, 11654−11657.
(65) Fang, R.; Zhang, H.; Yang, L.; Wang, H.; Tian, Y.; Zhang, X.; Jiang, L. Supramolecular Self-Assembly Induced Adjustable Multiple Gating States of Nanofluidic Diodes. *J. Am. Chem. Soc.* **2016**, *138*, 16372−16379.
(66) Traut, T. W. Physiological Concentrations of Purines and Pyrimidines. *Mol. Cell. Biochem.* **1994**, *140*, 1−22.
(67) Li, N.; Wang, X. Y.; Xiang, M. H.; Liu, J. W.; Yu, R. Q.; Jiang, J. H. Programmable Self-Assembly of Protein-Scaffolded DNA Nanohydrogels for Tumor-Targeted Imaging and Therapy. *Anal. Chem.* **2019**, *91*, 2610−2614.
(68) Geng, Y.; Zhong, Y.; Zhou, Q.; Chen, S.; Piao, Y.; Yin, W.; Lu, H.; Shen, Y. A Neutral Water-Soluble Mitochondria-Targeting Polymer. *Chem. Commun.* **2019**, *55*, 10015−10018.
(69) Irie, M.; Fukaminato, T.; Matsuda, K.; Kobatake, S. Photochromism of Diarylethene Molecules and Crystals: Memories, Switches, and Actuators. *Chem. Rev.* **2014**, *114*, 12174−12277.
(70) Feringa, B. L.; Jager, W. F.; Delange, B. Organic Materials for Reversible Optical Data Storage. *Tetrahedron* **1993**, *49*, 8267−8310.
(71) Irie, M.; Kunwatchakun, D. Photoresponsive Polymers: Reversible Photostimulated Dilation of Polyacrylamide Gels Having Triphenylmethane Leuco Derivatives. *Macromolecules* **1986**, *19*, 2476−2480.
(72) Yokoyama, Y. Fulgides for Memories and Switches. *Chem. Rev.* **2000**, *100*, 1717−1740.
(73) Feringa, B. L.; Van-Delden, R. A.; Koumura, N.; Geertsema, E. M. Chiroptical Molecular Switches. *Chem. Rev.* **2000**, *100*, 1789−1816.

https://doi.org/10.1021/acssensors.1c00463
ACS Sens. 2021, 6, 1529−1535